Journal of Vibration Engineering & Technologies (2024) 12:6437–6448
https://doi.org/10.1007/s42417-023-01261-4

ORIGINAL PAPER

Thomson Effect on an Initially Stressed Diffusive Magneto-thermoelastic Medium via Dual-Phase-Lag Model

Ebtesam E. M. Eraki[1] · Rania A. Fathy[1] · Mohamed I. A. Othman[1]

Received: 9 October 2023 / Revised: 18 November 2023 / Accepted: 17 December 2023 / Published online: 29 January 2024

Abstract

Objective This study investigates the influence of the Thomson effect on the behavior of a diffusive magneto-thermoelastic medium with initial stress and the dual-phase-lag (DPL) model.

Methods The normal mode analysis is utilized for solving the problem. The copper material was chosen for numerical assessments. The results are presented graphically for various physical quantities.

Results A comparison is made between the DPL model and the Lord and Shulman (L-S) theory, both in the absence and presence of the Thomson effect parameter as well as at two different values for the phase lag of heat flux.

Conclusions The findings provide insights into the impact of the Thomson effect on the behavior of the magneto thermoelastic medium, highlighting the differences between the DPL model and the L-S theory in different scenarios. This type of work has many applications in rock mechanics, geophysics, and petroleum industries. This work may be helpful for those researchers who are working in material science, smart materials, and new material designers.

Keywords Thomson effect · Diffusion · Initial stress · Normal mode method · Dual-phase-lag model

List of Symbols

$\boldsymbol{u}$	Mechanical displacement vector
T_0	Reference temperature
h	Magnetic field
H	Magnetic field intensity
ρ_e	Charge density
μ_0	Magnetic permeability of free space
ε_0	Electric permeability of free space
P	Chemical potential
$\beta_1 = (3\lambda + 2\mu)\alpha_t,\ \alpha_t$	Coefficient of linear thermal expansion
$\lambda,\ \mu$	Lame's constants
ρ	Density
τ_q	Phase-lag of the heat flux
k	Thermal conductivity
T	Absolute temperature
E	Induced electric field
C	Mass concentration
$\boldsymbol{J}$	Current density vector
σ_0	Electric conductivity
σ_{ij}	Stress tensor
ε_{ij}	Strain tensor
p	Initial stress
$\beta_2 = (3\lambda + 2\mu)\alpha_c,\ \alpha_c$	Coefficient of diffusion thermal expansion
μ	Chemical potential per unit mass
c_E	Specific heat at constant strain
τ_θ	The phase-lag of the temperature gradient
$a,\ b,\ d$	Are the coefficients describing the measure of thermal and diffusion effects
τ	Is the diffusion relaxation time which will ensure that the equation satisfied by the concentration will also predict finite speed of propagation of matter from one medium to another

✉ Mohamed I. A. Othman
m_i_a_othman@yahoo.com

Ebtesam E. M. Eraki
ebtesam.eraki@yahoo.com

Rania A. Fathy
raniafathy750@gmail.com

[1] Department of Mathematics, Faculty of Science, Zagazig University, P.O. Box 44519, Zagazig, Egypt

Introduction

The Lord–Shulman theory of thermoelasticity [1] with one relaxation time is based on the modification of the equation of heat conduction proposed by Maxwell [2] and later by Cattaneo [3]. This modification takes into account the time needed for the acceleration of heat flow. The theory ensures the finite speed of wave propagation of heat and displacement distributions. The remaining governing equations and constitutive relations for this theory are the same as those for the classical theory of thermoelasticity [4, 5].

In contrast, the DPL heat conduction equation includes two phase-lags in Fourier's law of heat conduction. This is done to account for microstructural effects that occur in high-rate heat transfer. The DPL model has been confirmed by experimental results [6] and has been shown to have physical meanings and applicability. Researchers such as Mukhopadhyay et al. [7], Othman and Eraki [8], and Abouelregal et al. [9] have further studied the effects of different fields on thermoelastic materials using the DPL model. These studies have looked at potential-temperature disturbances, gravity influence, and the inclusion of higher-order time-fractional derivatives in the equations. Overall, both the L-S theory and the DPL model provide valuable insights into thermoelasticity and have been utilized in various research studies on micro-elongated thermoelastic medium [10–25]

The Thomson effect is a significant phenomenon in the field of thermal power generation, particularly in electrical circuits and sensors. It occurs when an electric current flows through a circuit made of a single material that has a temperature difference along its length. This results in the evolution or absorption of heat. The transfer of heat due to the Thomson effect is in addition to the heat produced from the electrical resistance in conductors. It plays a crucial role in understanding and designing thermal power generation systems. Abouelregal and Abo-Dahab [26] conducted a study on the electro-magneto-thermoelastic problem in an infinitely solid cylinder using the dual-phase-lag model. This research aimed to analyze the Thomson effect in this specific context. Abd-Elaziz et al. [27, 28] also investigated multiple problems related to the Thomson effect and other effects on voids using the Green-Naghdi theories. Marin et al. [29] conducted research on mixed problems in thermoelasticity of type III for Cosserat media. These studies aimed to gain a deeper understanding of the Thomson effect's characteristics and its implications in various scenarios.

The diffusion phenomenon is of significant interest due to its numerous applications in geophysics and industries. Currently, the thermal diffusion process is being explored by oil companies for more efficient oil extraction from deposits. Kumar and Kansal [30] conducted research on the propagation of plane waves in a diffusive medium that is both isotropic and generalized thermoelastic. Recently, Othman et al. [31] examined the impact of fractional parameters on plane waves in a diffusive medium that is both generalized magneto-thermoelastic and dependent on reference temperature for elasticity. Othman et al. [32] also investigated the effect of magnetic field and thermal relaxation on the 2-D problem of generalized thermoelastic diffusion. Diffusion phenomena have many applications in geophysical and industrial (petroleum) areas. For instance, oil corporations have an interest in the thermo-diffusion technique to extract oil from oil resources with greater efficiency. Diffusion is employed in the manufacture of integrated circuits to introduce “dopants” into the semiconductor substrate in precise proportions. Diffusion is used in particular to dope polysilicon gates in MOS transistors, form integrated resistors, form the source/drain domains in MOS transistors, and form the base and emitter in bipolar transistors. The concentration in most of these applications is estimated using Fick’s law.

The initial stresses present in solids have a significant impact on how the material responds mechanically in situations where it is already stressed. These initial stresses are relevant in various fields including geophysics, engineering structures, and the behavior of soft biological tissues. These initial stresses occur as a result of processes like manufacturing or growth, and they exist even in the absence of external forces. Abd-Elaziz et al. [33] developed a formulation for initial stress in a thermo-porous elastic solid. Other researchers, such as Othman et al. [34–37], Singh et al. [38], Singh [39] and Ailawalia et al. [40], have applied this theory [33] to investigate plane harmonic waves within the framework of generalized thermoelasticity.

In this study, as a novelty of the previous works, we analyze the influence of the Thomson effect on diffusive media in the presence of initial stress, using the normal mode analysis method within the context of the DPL model.

Formulation of the Problem and Basic Equations

For two dimensional problem, assume the displacement vector as $\boldsymbol{u} = (u, 0, w)$, All quantities considered will be a function of the time variable t, and of the coordinates x and z. Consider a magnetic field with components $\boldsymbol{H} = (0, H_0, 0)$, having a constant intensity, which acts parallel to the direction of the y-axis, as shown in the schematic configuration of the problem (Fig. 1). The magnetic field of the for $\boldsymbol{H} \equiv (0, H_0 + h(x, z, t), 0)$ produces an induced electric field of components $\boldsymbol{E} \equiv (E_1, 0, E_3)$, and an induced magnetic

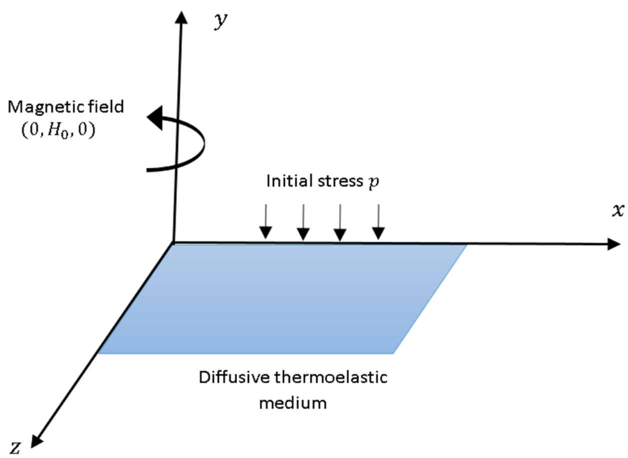

Fig. 1 The schematic configuration of the problem

field, as denoted by $\boldsymbol{h}$, and these satisfy the electromagnetism equations, in the linearized form.

The variation of magnetic and electric fields inside the medium is given by Maxwell's equations as follows Abd-Elaziz et al. [28]:

$$\nabla \times \boldsymbol{h} = \boldsymbol{J} + \boldsymbol{D}_{,t}, \tag{1}$$

$$\nabla \times \boldsymbol{E} = -\boldsymbol{B}_{,t}, \tag{2}$$

$$\nabla . \boldsymbol{B} = 0, \quad \nabla . \boldsymbol{D} = \rho_e, \tag{3}$$

$$\boldsymbol{B} = \mu_0(\boldsymbol{H} + \boldsymbol{h}), \quad \boldsymbol{D} = \varepsilon_0 \boldsymbol{E}. \tag{4}$$

The modified Ohm's law for a medium with finite conductivity supplements the above system of coupled equations, namely

$$\boldsymbol{J} = \sigma_0[\boldsymbol{E} + \mu_0\,(\boldsymbol{u}_{,t} \times \mathbf{H})]. \tag{5}$$

The constitutive relations in a homogeneous, isotropic thermoelastic solid can be written as Othman and Eraki [23]:

$$\sigma_{ij} = 2\mu\varepsilon_{ij} + (\lambda e - \beta_1\, T - \beta_2\, C)\delta_{ij} - p\,(\delta_{ij} + \omega_{ij}), \tag{6}$$

$$e_{ij} = \frac{1}{2}(u_{i,j} + u_{j,i}), \quad \omega_{ij} = \frac{1}{2}(u_{j,i} - u_{i,j}), \tag{7}$$

$$P = -\beta_2\, e + b\, C - a\, T. \tag{8}$$

The heat conduction equation (DPL) model can be written in the form (Othman and Eraki [35])

$$k\left(1 + \tau_\theta \frac{\partial}{\partial t}\right)\nabla^2 T = \left(1 + \tau_q \frac{\partial}{\partial t} + \frac{\tau_q^2}{2}\frac{\partial^2}{\partial t^2}\right)\left[\rho\, C_E T_{,t} + \left(\beta_1\, T_0 + M\right)e_{,t} + a\, T_0\, C_{,t}\right]. \tag{9}$$

where the term $M\, e_{,t}$ represents the Thomson effect.

The equation of mass diffusion is

$$d\,\beta_2\,\nabla^2 e + d\, a\,\nabla^2 T - d\, b\,\nabla^2 C + \left(1 + \tau\frac{\partial}{\partial t}\right) C_{,t} = 0. \tag{10}$$

The equations of motion, taking into consideration the Lorentz force, are

$$\sigma_{ji,j} + F_i = \rho\, u_{i,tt}. \tag{11}$$

The Lorentz force is given by [22–25]

$$\boldsymbol{F}_i = \mu_0(\boldsymbol{J} \times \boldsymbol{H})_{,i}. \tag{12}$$

The current density vector $\boldsymbol{J}$ is parallel to the electric intensity vector $\boldsymbol{E}$, thus $\boldsymbol{J} = (J_1, 0, J_3)$

The Ohm's law (5) after linearization gives (Abd-Elaziz et al. [33])

$$\boldsymbol{J} \equiv \sigma_0(E_1 - \mu_0 H_0 w_{,t},\ 0,\ E_3 + \mu_0 H_0 u_{,t}). \tag{13}$$

Equations (1), (4) and (13) give

$$\frac{\partial h}{\partial z} = -\sigma_0\,(E_1 - \mu_0\, H_0\, w_{,t}) - \varepsilon_0\, E_{1,t}\,, \tag{14}$$

$$\frac{\partial h}{\partial x} = \sigma_0\,(E_3 + \mu_0 H_0 u_{,t}) + \varepsilon_0 E_{3,t}. \tag{15}$$

From Eqs. (2) and (4), we get

$$\frac{\partial E_3}{\partial x} - \frac{\partial E_1}{\partial z} = \mu_0\, h_{,t}. \tag{16}$$

Using Eqs. (12) and (13), Lorentz force becomes

$$\boldsymbol{F} \equiv \mu_0 H_0 \sigma_0(-E_3 + \mu_0 H_0 u_{,t},\ 0,\ E_1 - \mu_0 H_0 w_{,t})\,, \tag{17}$$

From Eqs. (6), (7) and (17) in Eq. (11), equations of motion become

$$\begin{aligned}&\left(\mu - \frac{p}{2}\right)\nabla^2 u + \left(\lambda + \mu + \frac{p}{2}\right) e_{,x} - \beta_1 T_{,x}\\ &\quad - \beta_2 C_{,x} - \mu_0 H_0 \sigma_0 (E_3 + \mu_0 H_0 u_{,t}) = \rho\, u_{,tt},\end{aligned} \tag{18}$$

$$\begin{aligned}&\left(\mu - \frac{p}{2}\right)\nabla^2 w + \left(\lambda + \mu + \frac{p}{2}\right) e_{,z} - \beta_1 T_{,z} - \beta_2 C_{,z}\\ &\quad + \mu_0 H_0 \sigma_0 (E_1 - \mu_0 H_0 w_{,t}) = \rho\, w_{,tt}.\end{aligned} \tag{19}$$

For simplifying the governing equations, the following dimensionless quantities are proposed:

$$(x', z', u', w') = c_1\,\eta\,(x, z, u, w)\,,\quad T' = \frac{\beta_1}{(\lambda+2\,\mu)}\,T,\quad C' = \frac{\beta_2}{(\lambda+2\,\mu)}\,C,\quad \{\sigma'_{ij},\, p'\} = \frac{\{\sigma_{ij},\, p\}}{(\lambda+2\,\mu)}\,,$$
$$(t', \tau', \tau'_\theta, \tau'_q) = c_1^2\,\eta\,(t, \tau, \tau_\theta, \tau_q),\quad h' = \frac{\eta}{\sigma_0\,\mu_0\,H_0}h\,,\ P' = \frac{P}{\beta_2}, c_1^2 = \frac{\lambda+2\mu}{\rho}\,,\ \eta = \frac{\rho\,C_E}{k}\,. \tag{20}$$

For dimensionless sizes that are defined in Eq. (31), we can write the above basic equations in the following from, with dropping the dashed, for convenience

$$\left(\nabla^2 - a_1\frac{\partial}{\partial t} - \frac{\partial^2}{\partial t^2}\right)e - \nabla^2 T - \nabla^2 C - a_2 h_{,t} = 0, \tag{21}$$

$$\left(\nabla^2 - a_3\frac{\partial}{\partial t} - a_4\frac{\partial^2}{\partial t^2}\right)h - e_{,t} = 0, \tag{22}$$

$$\left(1+\tau_\theta\frac{\partial}{\partial t}\right)\nabla^2 T = \left(1+\tau_q\frac{\partial}{\partial t} + \frac{\tau_q^2}{2}\frac{\partial^2}{\partial t^2}\right)(T_{,t} + a_5\,C_{,t} + a_6\,e_{,t}), \tag{23}$$

$$\nabla^2 e + a_7\,\nabla^2 T - a_8\,\nabla^2 C + a_9\left(1+\tau\,\frac{\partial}{\partial t}\right)C_{,t} = 0, \tag{24}$$

where $a_i,\ (i = 1\,:\,9)$ are defined in the Appendix.

Normal Mode Analysis

The solution of physical variable may be analyzed modes as the following from

$$[e,\ T,\ h,\ C,\ \sigma_{ij}](x, z, t) = [e^*,\ T^*,\ h^*,\ C^*,\ \sigma_{ij}^*](z)\,e^{i(a_0\,x-\omega\,t)}, \tag{25}$$

where ω is a complex constant, $i = \sqrt{-1}$, a_0 is wave number in x-direction.

Using Eq. (25) into Eqs. (21)–(24), then we get

$$(D^2 - b_1)\,e^* - (D^2 - a_0^2)\,T^* - (D^2 - a_0^2)\,C^* + b_2 h^* = 0, \tag{26}$$

$$b_3\,e^* + (D^2 - b_4)\,h^* = 0\,, \tag{27}$$

$$-\,b_6 e^* + (D^2 - b_7)\,T^* - b_8 C^* = 0\,, \tag{28}$$

$$(D^2 - a_0^2)\,e^* + a_7(D^2 - a_0^2)T^* - (a_8 D^2 - b_9)\,C^* = 0\,. \tag{29}$$

Equations (26)–(29) have a non-trivial solution if the physical quantities determinant coefficients equal to zero, then we get:

$$(D^8 - A_1\,D^6 + A_2\,D^4 - A_3\,D^2 + A_4)\{e^*, h^*, T^*, C^*\} = 0\,. \tag{30}$$

Equation (30) can be factorized as

$$(D^2 - K_1^2)(D^2 - K_2^2)(D^2 - K_3^2)(D^2 - K_4^2)\,\{e^*,\, h^*,\, T^*,\, C^*\} = 0\,, \tag{31}$$

where, $K_n^2, (n = 1,\ 2,\ 3, 4)$ are roots of Eq. (31).

The general solution of Eq. (40) bounded as $z \to \infty$ is given by

$$(e^*,\ h^*,\ T^*,\ C^*)(z) = \sum_{n=1}^{4}(1,\ H_{1n},\ H_{2n},\ H_{3n})R_n\,e^{-k_n z}. \tag{32}$$

Substituting from Eqs. (20), (25) and (32) into Eq. (6), we get

$$\sigma = \sum_{n=1}^{4} H_{4n}\,R_n\,e^{(-k_n z + i\,a_0\,x - i\,\omega\,t)} - p, \tag{33}$$

$$P^* = \sum_{n=1}^{4} H_{5n}\,R_n\,e^{-k_n z}. \tag{34}$$

where $b_i,\ (i = 1-9)$ and $H_{jn},\ (j = 1-5)$ are defined in Appendix.

The Boundary Conditions

The parameters $R_n, (n = 1, 2, 3, 4)$ have to be selected such that boundary conditions at the surface $z = 0$ are

$$e^* = 0,\qquad h^* = h_0\,,\qquad T^* = 0\,,\qquad \frac{\partial C^*}{\partial z} = 0. \tag{35}$$

Applying boundary conditions (35), using Eq. (32), we obtain a system of equations, by solving this system using matrix inverse, the constants $R_n, (n = 1, 2, 3, 4)$ are obtained as follows

$$\begin{pmatrix} R_1 \\ R_2 \\ R_3 \\ R_4 \end{pmatrix} = \begin{pmatrix} 1 & 1 & 1 & 1 \\ H_{11} & H_{12} & H_{13} & H_{14} \\ H_{21} & H_{22} & H_{23} & H_{24} \\ -k_1\,H_{31} & -k_2\,H_{32} & -k_3\,H_{33} & -k_4\,H_{34} \end{pmatrix}^{-1} \begin{pmatrix} 0 \\ h_0 \\ 0 \\ 0 \end{pmatrix}. \tag{36}$$

Numerical Analysis and Discussion

The copper substance was selected for numerical evaluations. The problem's material constants were then taken as (Abd-Elaziz et al. [28]).

$\lambda = 7.76 \times 10^{10}\,\mathrm{N.m^{-2}}$, $\mu = 3.86 \times 10^{10}\,\mathrm{kg.m^{-1}.s^{-2}}$, $K = 386\,\mathrm{w.m^{-1}.k^{-1}}$, $T_0 = 293$ K,

$\alpha_t = 1.78 \times 10^{-5}\,\mathrm{k^{-1}}$, $\alpha_c = 1.98 \times 10^{-4}\,\mathrm{k^{-1}}$, $\rho = 8954\,\mathrm{kg.m^{-3}}$, $C_e = 383.1\,\mathrm{J.kg^{-1}.k^{-1}}$, $\sigma_0 = 9.36 \times 10^5$ siemens $\mathrm{m^{-1}}$.

The comparisons were carried out for:

$$x = 0.83\ \mathrm{m},\quad t = 0.05\,\mathrm{s},\quad \tau_T = 0.0001\,\mathrm{s},$$
$$\tau_q = 0.015\,\mathrm{s},\quad \omega = \omega_0 + i\,\omega_1,\quad \omega_0 = 0.1\,\mathrm{s^{-1}},$$
$$\omega_1 = 0.000\,\mathrm{s^{-1}},\ H_0 = 55\mathrm{A\,m^{-1}},\ M = 2\,\mathrm{N\,m^{-2}}.$$

The numerical values, outlined above, were used for the distribution of the physical quantities T, h, σ, e, c, p, for the problem have established in the context of DPL model and L-S theory, in the absence and presence of Thomson effect parameter ($M = 0, 2$).

In these figures, the dotted line represents the solution in the DPL model in the presence of Thomson effect parameter, the dashed-dotted line represents the solution derived using DPL model in the absence of Thomson effect parameter, the solid line indicates the (L-S) theory in the presence of Thomson effect parameter and finally the dashed line refers to (L-S) theory when Thomson effect parameter equals zero. Here all variables are taken in non-dimensional form. The results were obtained by using MATLAB 2021a.

Figures 2, 3 and 4 depict that the distribution of the strain distribution e, temperature T and the stress distribution σ, they show that they have the same behavior, they are noticed that their values increases to a maximum value in the range $0 \le z \le 1$, then decreases until become constant in the range $1 \le z \le 12$, this results for L-S theory and DPL model. The values of these physical quantities in the presence of the Thomson effect parameter ($M = 2$) for L-S theory are greater than in the absence of it ($M = 0$), but the reversed behavior is found for DPL model. Farther more the values in the context of L-S theory are higher than those for DPL model. Figure 5 illustrates the dispersion of the generated magnetic field h. It shows that the impact of the Thomson parameter on the induced magnetic field is insignificant. Figures 6 and 7 show the distribution of concentration C and chemical potential P. Then value of C decrease to a minimum value in the interval $0 \le z \le 7$, and finally up to zero in $7 \le z \le 12$, while the values of P decrease to a minimum value in the interval $0 \le z \le 5$, and finally remains constant and up to zero in $5 \le z \le 12$. In the context of L-S theory, the values of concentration and chemical potential are higher in the presence of the Thomson effect parameter ($M = 2$) compared to its absence ($M = 0$). However, the behavior is reversed for the DPL model when compared to L-S theory. Additionally, the values in the context of L-S theory are higher than those for the DPL model. Figures 8, 9, and 10 demonstrate the distribution of strain e, temperature T, and stress σ in the presence of the Thomson effect parameter ($M = 2$) and at different values of the phase lag of heat flux $\tau_q (\tau_q = 0.015, 0.04)$. They show the same behavior for both L-S theory and DPL model, with values increasing to a maximum in the range $0 \le z \le 1$, and then decreasing until they become constant in the range $1 \le z \le 12$. It show that the values of those quantities at $\tau_q = 0.04$ are higher than the previous distributions at $\tau_q = 0.015$. Additionally, the values in the context of L-S theory are higher than those for the DPL model. Figure 11 shows that the induced magnetic field almost does not change from $\tau_q = 0.015$ to $\tau_q = 0.04$. Figures 12 and 13 explain the distributions of the chemical potential P and the concentration C in the context of the two theories for ($\tau_q = 0.015, 0.04$) and in the presence of the Thomson effect parameter ($M = 2$). The values of C are decreased to a minimum value in the interval $0 \le z \le 7$, and finally up to zero in $7 \le z \le 12$, while the values of P are decreased to a minimum value in the interval $0 \le z \le 5$, and finally remains constant and up to zero in $5 \le z \le 12$. It disappear that the values of those quantities at $\tau_q = 0.04$ are greater than those

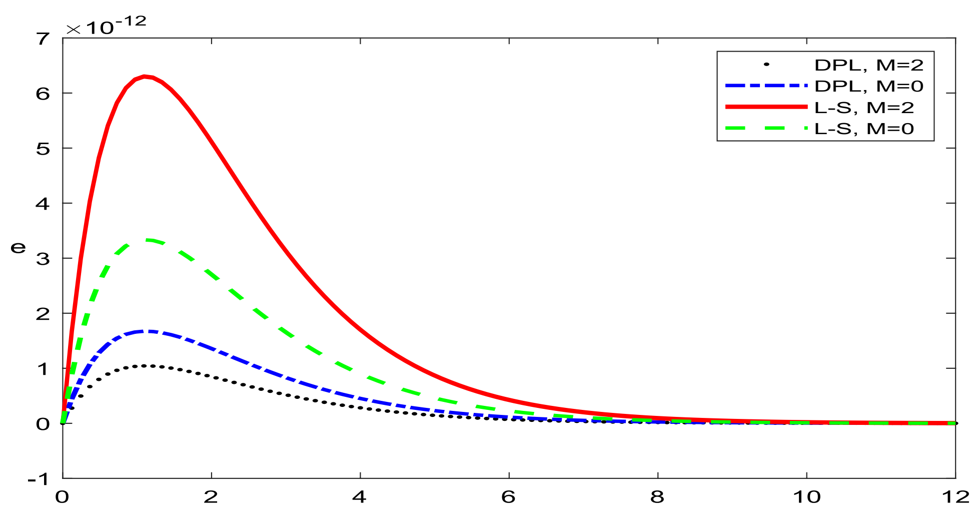

Fig. 2 The variation of strain field distribution with distance z for different values of Thomson effect parameter $M = 0, 2$

at $\tau_q = 0.015$. Also, the values in the context of L-S theory are higher than those for DPL model for ($\tau_q = 0.015\,, 0.04$).

3D curves in Figs. 14, 15 and 16 demonstrate the relationship between physical quantities and both distance components (x, z) in the context of the DPL model. These figures are.

important for studying the dependence of physical quantities on the vertical component of distance. The curves show wave propagation and indicate a strong dependence on the vertical distance.

Conclusion

By comparing the figures that were obtained, important phenomena are observed:

1. The phenomenon of finite speeds of propagation is manifested in all figures.
2. All physical quantities satisfied the boundary conditions.
3. The Thomson effect parameter has a noticeable influence on all physical quantities (except the induced magnetic field). It decreases them under both DPL model and L-S theory.
4. The values of most physical quantities in the context of L-S theory are higher than those for the DPL model, in the presence and absence of the Thomson effect parameter as well as at different values of the phase lag of the heat flux.

Appendix

$$a_1 = \frac{\mu_0^2 H_0^2 \sigma_0}{\eta \rho c_1^2}, a_2 = \frac{\mu_0^3 H_0^2 \sigma_0^2}{\eta^2 \rho c_1^2}, a_3 = \frac{\sigma_0 \mu_0}{\eta},$$

$$a_4 = \varepsilon_0 \mu_0 c_1^2, a_5 = \frac{a T_0 \beta_1}{\eta \beta_2 K}, a_6 = \frac{\beta_1(\beta_1 T_0 + M)}{K\eta(\lambda + 2\mu)},$$

$$a_7 = \frac{a\,(\lambda + 2\,\mu)}{\beta_1\ \beta_2}\ , \quad a_8 = \frac{b\,(\lambda + 2\,\mu)}{\beta_2^2}\ ,$$

$$a_9 = \frac{(\lambda + 2\,\mu)}{d\,\eta\ \beta_2^2}\ , \quad a_{10} = \frac{(3\lambda + 2\,\mu)}{3(\lambda + 2\,\mu)}\ ,$$

$$b_1 = a_0^2 - i\,a_1\,\omega - \omega^2, b_2 = i a_2 \omega, \quad b_3 = i\omega\ , \ b_4 = a_0^2 - i\omega\,a_3 - a_4\omega^2,$$

$$b_5 = \frac{-\,i\omega\,(1 - i\omega\tau_q - \frac{\omega^2}{2}\tau_q^2)}{(1 - i\omega\tau_\theta)}, b_6 = b_5\,a_6, b_7 = a_0^2 + b_5\ , b_8 = a_5\ b_5,$$

$$b_9 = a_8 a_0^2\ - i\omega\,a_9(1 - i\omega\,\tau),$$

$$A_1 = \frac{1}{(a_8 - 1)}\left[a_8(b_1 + b_6 + b_7) + b_9 + (1 + a_7)b_8 - b_7 + a_7 b_6 - 2a_0^2 + b_4(a_8 - 1)\right],$$

$$A_2 = \frac{1}{(a_8 - 1)}\{\ b_9\,(b_6 + b_7) + a_0^2\,b_8(1 + a_7) + (b_1 + b_4)(a_8\,b_7 + b_9 + a_7\,b_8) + a_0^2(a_8\,b_6 + b_8) - 2\,a_0^2(b_7 - a_7\,b_6) - a_0^4 + b_4(a_8\,b_1 + a_8\,b_6 + b_8 - b_7 + a_7\,b_6 - 2\,a_0^2) - a_8\,b_2\,b_3\},$$

$$A_3 = \frac{1}{(a_8 - 1)}\{(b_1 + b_4)(b_7 b_9 + a_0^2 a_7 b_8) + a_0^2(b_6 b_9 + a_0^2 b_8) - a_0^4(b_7 - a_7 b_6) - b_2 b_3(a_8 b_7 + b_9 + a_7 b_8) + b_4[a_8 b_1 b_7 + b_1 b_9 + a_7 b_1 b_8 + b_6 b_9 + a_0^2 b_8 + a_0^2(a_8 b_6 + b_8) - 2\,a_0^2(b_7 - a_7 b_6) - a_0^4]\},$$

$$A_4 = \frac{1}{(a_8 - 1)}[(b_1 b_4 - b_2 b_3)(b_7 b_9 + a_0^2 a_7 b_8) + a_0^2 b_4(b_6 b_9 + a_0^2 b_8 - a_0^2 b_7 + a_0^2 a_7 b_6)],$$

$$H_{1n} = \frac{b_3}{b_4 - k_n^2}\ , H_{2n} = \left[\frac{[(b_8 + a_8\,b_6)\,k_n^2 - (a_0^2\,b_8 + b_6\,b_9)]}{a_8\,k_n^4 - (a_8\,b_7 + b_9 + a_7\,b_8)\,k_n^2 + (b_7\,b_9 + a_0^2\,a_7\,b_8)}\right],$$

$$H_{3n} = \frac{1}{b_8}[(k_n^2 - b_7)H_{1n} - b_6]\ , H_{4n} = a_{10} - H_{2n} - H_{3n}, H_{5n} = -1 + a_8\ H_{3n} - a_7\ H_{2n}\ .$$

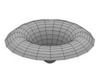

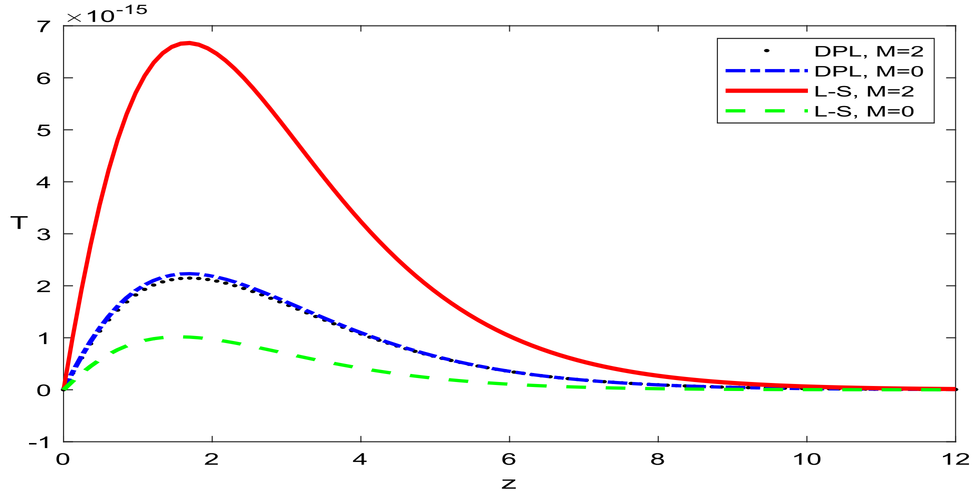

Fig. 3 The variation of temperature field distribution with distance z for different values of Thomson effect parameter $M = 0,\ 2$

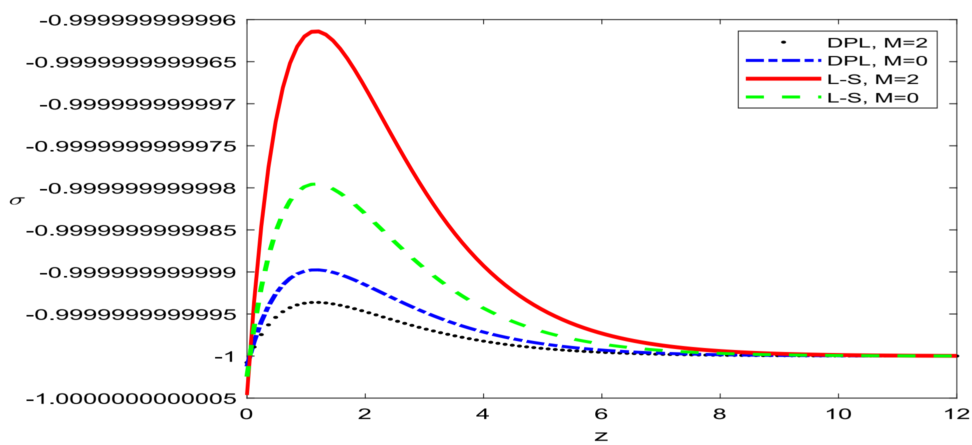

Fig. 4 The variation of stress field distribution with distance z at different values of Thomson effect parameter $M = 0,\ 2$

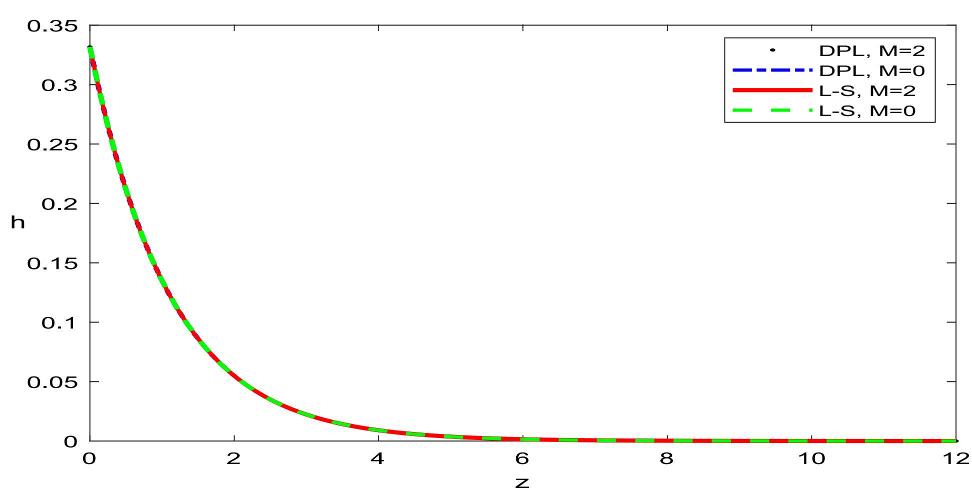

Fig. 5 The variation of induced magnetic field distribution with distance z for different values of Thomson effect parameter $M = 0,\ 2$

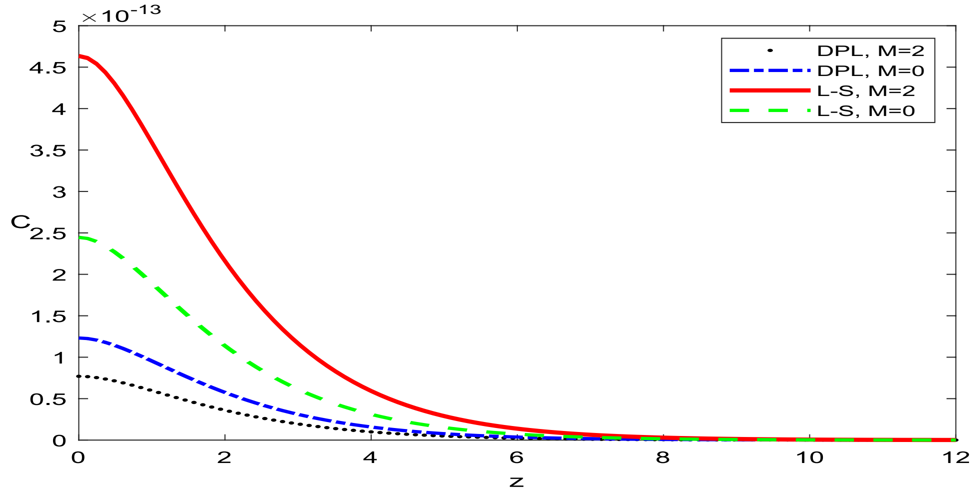

Fig. 6 The variation of concentration field distribution with distance z for different values of Thomson effect parameter $M = 0,\ 2$

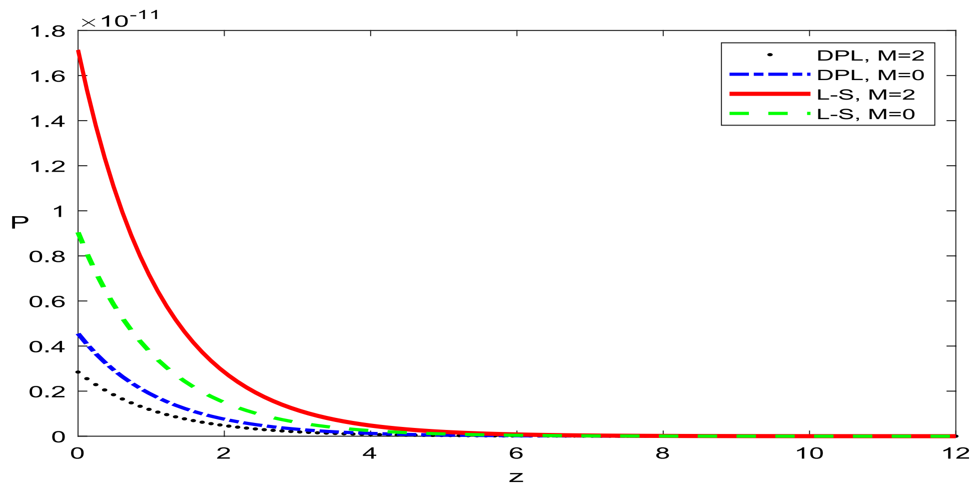

Fig. 7 The variation of chemical potential field distribution with distance z for different values of Thomson effect parameter $M = 0,\ 2$

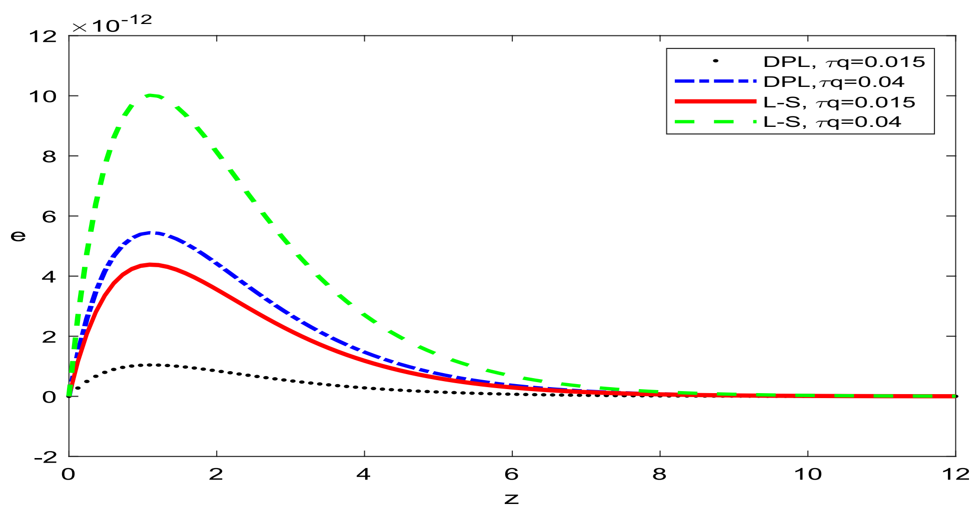

Fig. 8 The variation of strain field distribution with distance z for different values of τ_q at $M = 2$

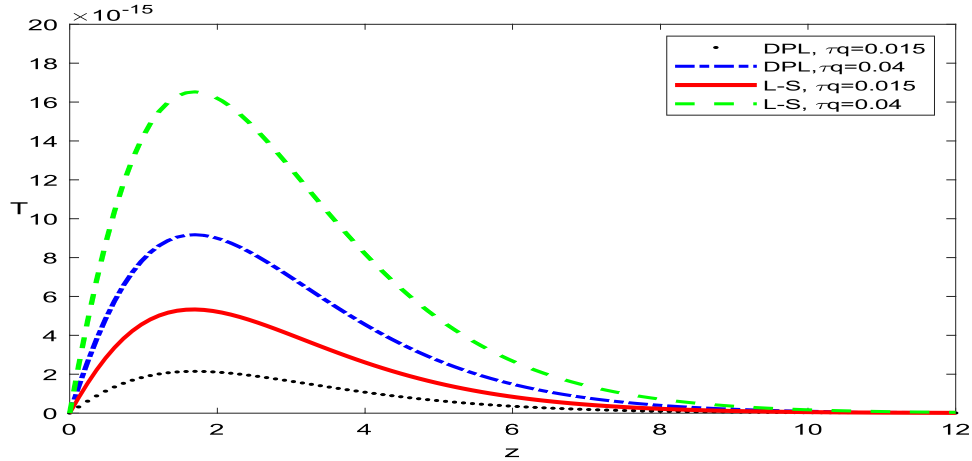

Fig. 9 The variation of temperature field distribution with distance z for different values of τ_q at $M = 2$

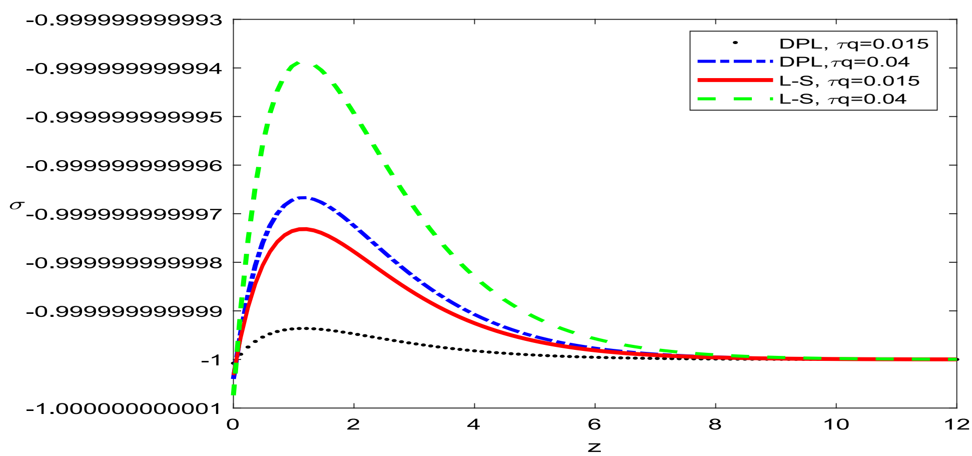

Fig. 10 The variation of stress field distribution with distance z for different values of τ_q at $M = 2$

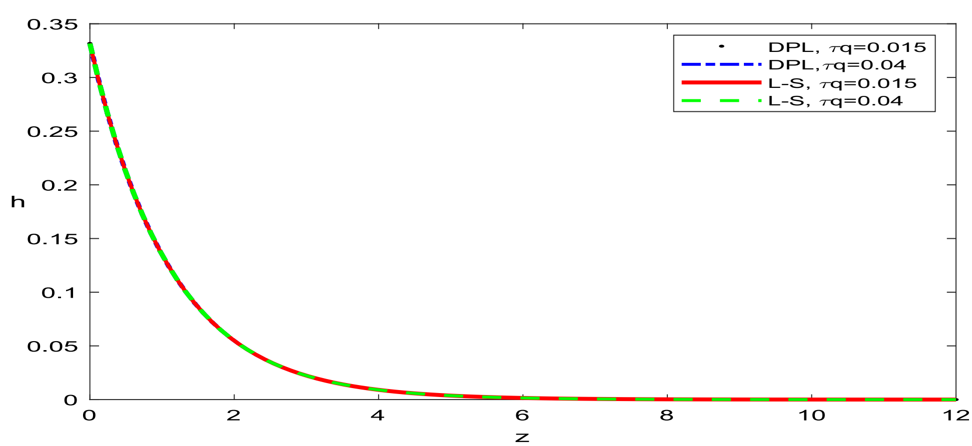

Fig. 11 The variation of induced magnetic field distribution with distance z for different values of τ_q at $M = 2$

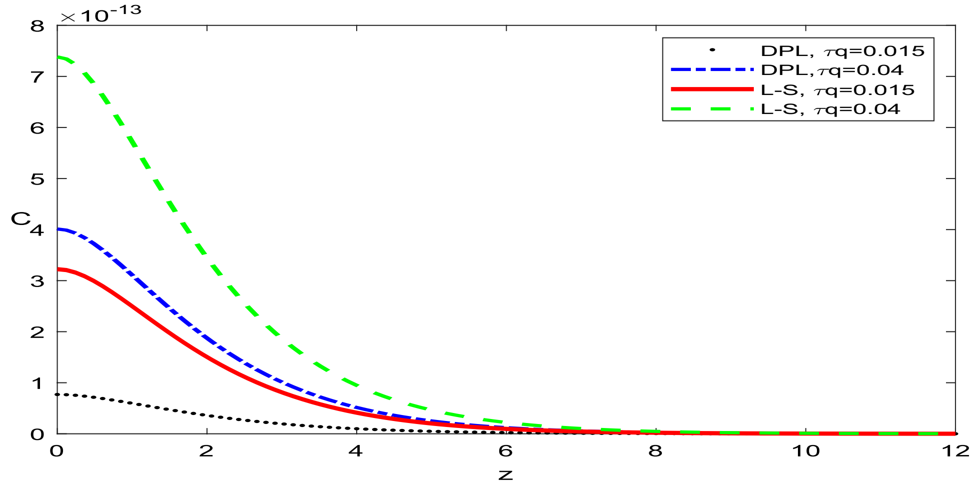

Fig. 12 The variation of concentration field distribution with distance z for different values of τ_q at $M = 2$

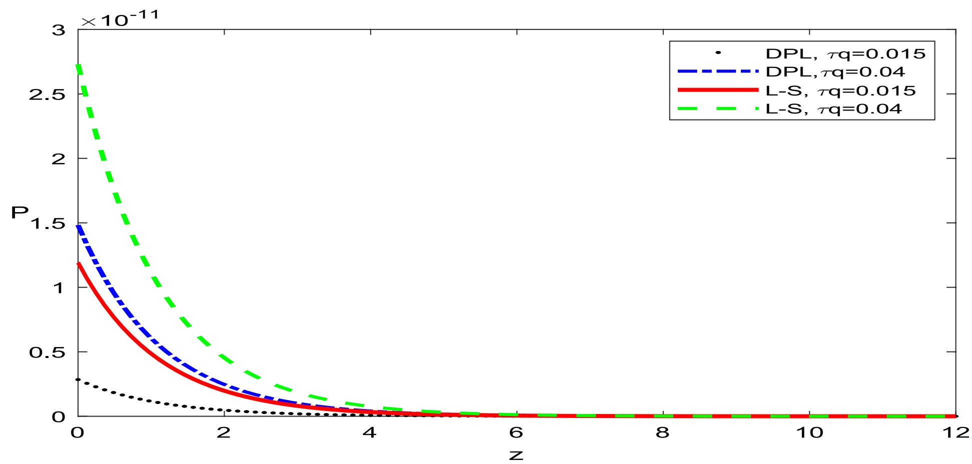

Fig. 13 The variation of chemical potential field distribution with distance z for different values of τ_q at $M = 2$

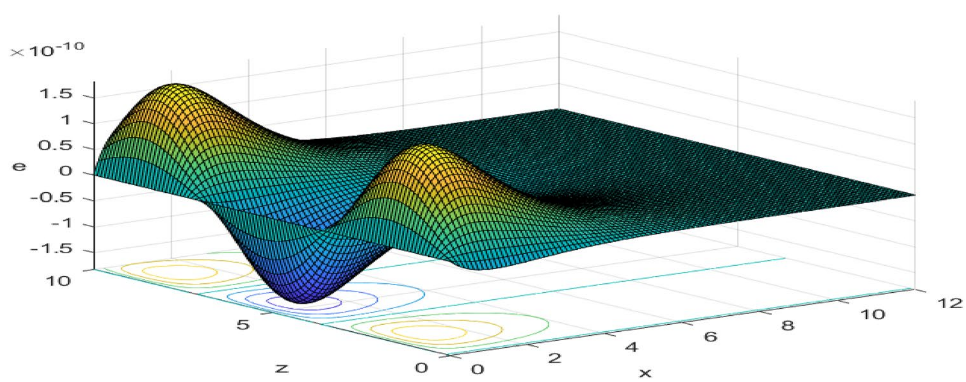

Fig. 14 (3D) Strain distribution e against both components of distance x, z based on DPL model in the presence of Thomson effect parameter $M = 2$

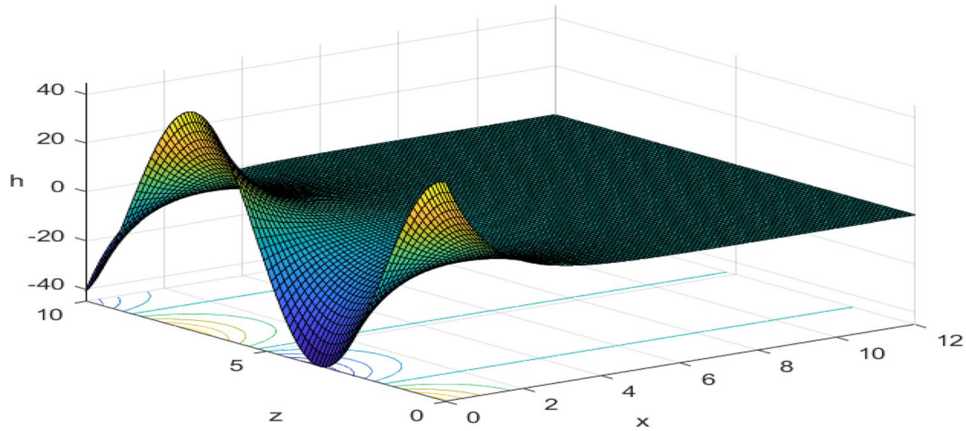

Fig. 15 (3D) Induced magnetic field distribution h against both components of distance $x,\ z$ based on DPL model in the presence of Thomson effect parameter $M = 2$

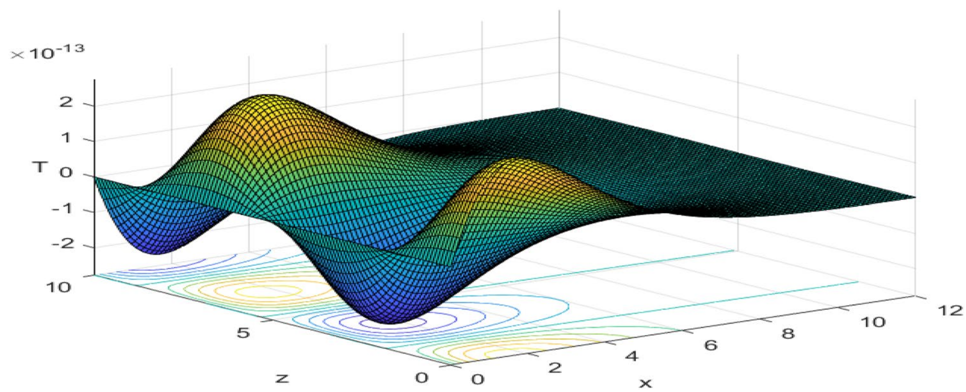

Fig. 16 (3D) Temperature distribution T against both components of distance $x,\ z$ based on DPL model in the presence of Thomson effect parameter $M = 2$

Author Contributions The authors contributed equally to this work and approved it for publication.

Funding Open access funding provided by The Science, Technology & Innovation Funding Authority (STDF) in cooperation with The Egyptian Knowledge Bank (EKB). There is no funding available for this research article.

Data Availability Data sharing is not applicable to this paper as no data sets were created or analyzed during the current investigation.

Declarations

Conflict of Interest The authors confirm that they have no known competing financial interests or personal relationships that could have appeared to influence the work presented in this paper. On behalf of all authors, the corresponding author states that there is no conflict of interest.

References

1. Lord HW, Shulman Y (1967) A generalized dynamical theory of thermoelasticity. J Mech Phys of Sol 15:299–309. https://doi.org/10.1016/0022-5096(67)90024-5
2. Maxwell JC (1867) On the dynamical theory of gases. J Philos Trans R Soc Lond 157:49–88. https://www.jstor.org/stable/108958
3. Cattaneo C (1948) Sulla conduzione del calore. Atti del Seminario Matematico Fisicodella Università di Modena 3:83–101. https://doi.org/10.1007/978-3-642-11051-1_5
4. Tzou DY (1996) Macro-to micro-scale heat transfer: the lagging behavior, 1st edn. Taylor & Francis, Washington
5. Tzou DY (1995) A unified approach for heat conduction from macro-to micro-scales. J Heat Transfer 117:8–16
6. Tzou DY (1995) Experimental support for the lagging behavior in heat propagation. J Thermophys Heat Transfer 9:686–693
7. Mukhopadhyay S, Kothari S, Kumar R (2011) A domain of influence theorem for thermoelasticity with dual-phase-lags. J Therm Stress 34:923–933. https://doi.org/10.1080/01495739.2011.601257
8. Othman MIA, Eraki EEM (2018) Effect of gravity on generalized thermoelastic diffusion due to laser pulse using dual-phase-lag model. Multi Model Mater Struct 14(3):457–481. https://doi.org/10.1108/MMMS-08-2017-0087

9. Abouelregal AE, Elhagary MA, SoleimanA KKM (2022) Generalized thermoelastic-diffusion model with higher-order fractional time derivatives and fourphase-lags. Mech Based Design Struct Mach 50:897–914. https://doi.org/10.1080/15397734.2020.1730189
10. Othman MIA, Atwa SY, Eraki EEM, Ismail MF (2021) The initial stress effect on a thermoelastic micro-elongated solid under the dual-phase-lag model. Appl Phys A 127:697. https://doi.org/10.1007/s00339-021-04809-x
11. Othman MIA, Atwa SY, Eraki EEM, Ismail MF (2021) A thermoelastic micro-elongated layer under the effect of gravity in the context of the dual-phase lag model. ZAMM 101(12):e202100109. https://doi.org/10.1002/zamm.202100109
12. Zenkour AM (2020) Magneto-thermal shock for a fiber-reinforced anisotropic half-space studied with a refined multi-dual-phase-lag model. J Phys Chem Sol 137:109213. https://doi.org/10.1016/j.jpcs.2019.109213
13. Dahab SM, Abouelregal AE, Marin M (2020) Generalized thermoelastic functionally graded on a thin slim strip non-Gaussian laser beam. Symmetry 12(7):Art. No. 1094. https://doi.org/10.3390/sym12071094
14. Abbas IA, Hobiny A, Marin M (2020) Photo-thermal interactions in a semi-conductor material with cylindrical cavities and variable thermal conductivity. J Taibah Univ Sci 14(1):1369–1376. https://doi.org/10.1080/16583655.2020.1824465
15. Zenkour AM, Saeed T, Aati AM (2023) Refined dual-phase-lag theory for the 1D behavior of skin tissue under Ramp-type heating. Materials 16(6):2421. https://doi.org/10.3390/ma16062421
16. Kutbi MA, Zenkour MA (2022) Refined dual-phase-lag Green-Naghdi models for thermoelastic diffusion in an infinite medium. Waves Random Complex Media 32(2):947–967. https://doi.org/10.1080/17455030.2020.1807073
17. Salem A (2020) Thermo-diffusion of solid cylinders based upon refined dual-phase-lag models. Multi Model Mater Struct 16(6):1417–1434. https://doi.org/10.1108/MMMS-12-2019-0213
18. Zenkour AM (2020) Thermoelastic diffusion problem for a half-space due to a refined dual-phase-lag Green-Naghdi model. J Ocean Eng Sci 5(3):214–222. https://doi.org/10.1016/j.joes.2019.12.001
19. Zenkour AM, El-Shahrany HD (2020) Vibration suppression of magnetostrictive laminated beams resting on viscoelastic foundation. Appl Math Mech 41:1269–1286. https://doi.org/10.1007/s10483-020-2635-7
20. Fahmy MA, Elmehmadi MM (2023) Fractional dual-phase-lag model for nonlinear visco-elastic soft tissues. Fractal Fract 7(1):66. https://doi.org/10.3390/fractalfract7010066
21. Fahmy MA (2021) A new boundary element algorithm for a general solution of nonlinear space-time fractional dual-phase-lag bio-heat transfer problems during electro-magnetic radiation. Case Stud Therm Eng 25:100918. https://doi.org/10.1016/j.csite.2021.100918
22. Abd-Alla A, El-Naggar AM, Fahmy MA (2003) Magneto-thermoelastic problem in non-homogeneous isotropic cylinder. Heat Mass Transf 39(7):625–629. https://doi.org/10.1007/s00231-002-0370-3
23. Fahmy MA (2013) Implicit–explicit time integration DRBEM for generalized magneto-thermoelasticity problems of rotating anisotropic viscoelastic functionally graded solids. Eng Anal Bound Elem 37(1):107–115. https://doi.org/10.1016/j.enganabound.2012.08.002
24. Fahmy MA (2018) Shape design sensitivity and optimization for two-temperature generalized magneto-thermoelastic problems using time-domain DRBEM. J Therm Stress 41(1):119–138. https://doi.org/10.1080/01495739.2017.1387880
25. Fahmy MA, Elmehmadi MM (2022) Boundary element analysis of rotating functionally graded anisotropic fiber-reinforced magneto-thermoelastic composites. Open Eng 12(1):313–322. https://doi.org/10.1515/eng-2022-0036
26. Abouelregaland AE, Abo-Dahab SM (2014) Dual-phase-lag diffusion model for Thomson's phenomenon on electromagneto-thermoelastic an infinitely long solid cylinder. J Comput Theor Nanosci 11:1031–1039. https://doi.org/10.1166/jctn.2014.3459
27. Abd-Elaziz EM, Othman MIA (2019) Effect of Thomson and thermal loading due to laser pulse in a magneto-thermoelastic porous medium with energy dissipation. ZAMM 99(8):e201900079. https://doi.org/10.1002/zamm.201900079
28. Abd-Elaziz EM, Marin M, Othman MIA (2019) On the effect of Thomson and initial stress in a thermo-porous elastic solid under G-N electromagnetic theory. Symmetry 11(3):413. https://doi.org/10.3390/sym11030413
29. Marin M, Seadawy A, Vlase S, Chirila A (2022) On mixed problem in thermo-Elasticity of type III for Cosserat media. J Taibah Univ Sci 16(1):1264–1274. https://doi.org/10.1080/16583655.2022.2160290
30. Kumar R, Kansal T (2012) Plane waves and fundamental solution in the generalized theories of thermoelastic diffusion. Int J Appl Math Mech 8(4):1–20. https://doi.org/10.18720/MPM.3512018_13
31. Othman MIA, Sarkar N, Atwa SY (2013) Effect of fractional parameter on plane waves of generalized magneto–thermoelastic diffusion with reference temperature-dependent elastic medium. Comp Math Appl 65(7):1103–1118. https://doi.org/10.1016/j.camwa.2013.01.047
32. Othman MIA, Farouk RM, Hamied HA (2013) The effect of magnetic field and thermal relaxation on 2-D problem of generalized thermoelastic diffusion. Int Appl Mech 49(2):245–255. https://doi.org/10.1007/s10778-013-0564-z
33. Abd-Elaziz EM, Marin M, Othman MIA (2019) On the effect of Thomson and initial stress in a thermo-porous elastic solid under G-N electromagnetic theory. Appl Continu Mech 11(3):413–430. https://doi.org/10.3390/sym11030413
34. Abbas IA, Othman MIA (2012) Generalized thermoelastic interaction in a fiber-reinforced anisotropic half-space under hydrostatic initial stress. J Vib Control 18(2):175–182. https://doi.org/10.1177/1077546311402529
35. Othman MIA, Eraki EEM (2017) Generalized magneto-thermoelastic half-space with diffusion under initial stress using three-phase-lag model. Based Design Struct Mach Int J 45(2):145–159. https://doi.org/10.1080/15397734.2016.1152193
36. Othman MIA, Abo-Dahab SM, Alsubeai ONS (2017) Reflection of plan waves from a rotating magneto-thermoelastic medium with two-temperature and initial stress under three theories. Mech Mech Eng 21(2):217–232
37. Othman MIA, Fekry M, Marin M (2020) Plane waves in generalized magneto-thermo-viscoelastic medium with voids under the effect of initial stress and laser pulse heating. Struct Eng and Mech An Int'l J 73(6):621–629. https://doi.org/10.12989/sem.2020.73.6.621
38. Singh B, Kumar A, Singh J (2006) Reflection of generalized thermoelastic waves from a solid half-space under hydrostatic initial stress. Appl Math Comput 177(1):170–177. https://doi.org/10.1016/j.amc.2005.10.045
39. Singh B (2008) Effect of hydrostatic initial stresses on waves in a thermoelastic solid half-space. Appl Math Comp 198:494–505. https://doi.org/10.1016/j.amc.2007.08.072
40. Ailawalia P, Kumar S, Khurana G (2009) Deformation in a generalized thermo-elastic medium with hydrostatic initial stress subjected to different sources. Mech and Mech Eng 13(1):5–24